

Simulation of contact forces and contact characteristics during meshing of elastic beveloid gears

Trong Phu Do, Pascal Ziegler, Peter Eberhard

Institute of Engineering and Computational Mechanics, University of Stuttgart

Pfaffenwaldring 9, 70569 Stuttgart, Germany

e-mail: [trongphu.do, pascal.ziegler, peter.eberhard]@itm.uni-stuttgart.de

Beveloid gears, also known as conical involute gears with very complex tooth shapes, gain more and more importance in industrial practice due to their ability to realize gear stages with crossed axes. This is why they are frequently found in power transmissions. The most familiar application of beveloid gears is the reduction gear used in marine transmissions, but in the last few years they have also been used increasingly often in the automotive industry. In the last decade many studies on beveloid gears were published, however, the meshing between teeth and the contact characteristics during meshing of beveloid gears still have not been studied in detail using fully elastic models.

In this work, the fully elastic multibody approach will be applied to study contact forces and contact characteristics including contact patterns during meshing of straight beveloid gears. To validate the fully elastic approach, simulation results of a beveloid gear pair by finite element method and by the fully elastic multibody system are compared. The comparison shows very good agreement.

Keywords: multibody dynamics, gears, involute gears, beveloid gears, contact forces, contact patterns, elastic multibody system.

1. INTRODUCTION

The behavior of beveloid gears is not as well understood as the behavior of spur or bevel gears. Theoretically, the bearing contacts of beveloid gears as rigid bodies under non-parallel axes meshing are point contacts. For flexible bodies, the contact areas will enlarge to ellipses but still the contact ellipses are relatively small leading to a low durability of tooth surfaces because of high contact stresses. Investigations of contact ellipses can be found in [1, 2], but these studies are done only with mathematical models of rigid gear bodies. The publications [3–6] introduced the contact stress of straight and helical beveloid gear pairs as fully elastic models, but the analyses were established only by a finite element (FE) model of one pair of contact teeth of the gear pairs with a relatively small contact area. The contact was calculated only at the middle of the tooth flanks. The meshing between teeth and the contact characteristics during meshing still have not been studied in detail. In particular, the contact behavior has not yet been studied with a fully elastic model for several consecutive contacts including dynamical effects.

Very precise simulations of contact forces between gears and beveloid gears require a fully elastic description. Unfortunately, the simulation of full meshing cycles and many contacts is practically infeasible using full finite element models. One very efficient way to dynamically simulate fully elastic gears is to use a modally reduced elastic multibody system (EMBS) with a nodal-based algorithm. For the contact calculation a node-to-segment penalty formulation and a coarse collision detection are introduced and the differential equations of motion are integrated using an explicit time integration scheme. This approach was already successfully applied to spur gears. In order to investigate full meshing cycles of beveloid gears, in this work this approach is extended for the complicated geometry of beveloid gears. The EMBS approach will be used to simulate the contact

forces and contact behaviors of straight beveloid gears for full meshing cycles and many contacts. The contact forces between a very precise nonlinear FE model and the proposed fully elastic model will be shown and compared, then the contact forces and contact characteristics including contact patterns during meshing of a very large rotational angle will be simulated and discussed. The efficiency of gear flank corrections in elastic simulations is also investigated and presented using the new approach.

2. ELASTIC MULTIBODY MODEL

In this section, the description of gear wheels as elastic multibody models is introduced and the modal reduction is explained. The contact algorithm and some simulation results are given in the subsections. For a detailed description, we refer to [7–9].

2.1. Description of an elastic gear

To overcome the large integration times of dynamic FE simulation while still having an accurate model, a modally reduced model is used in this work. Usually, the deformations of gears are small and can be described by a linear theory. However, the main application of gears includes large rotations which are nonlinear by nature. Otherwise, most reduction techniques are based on linear methods, see [10, 11]. One way to apply linear reduction methods despite the large rotations is to use a floating frame of reference formulation, described in detail in [7, 8]. This method is especially well-suited for problems with a large movement of the reference frame and only small elastic deformations.

The basic idea of the floating frame of reference is the separation of the overall motion of a single flexible body into a usually nonlinear describable motion of the reference frame and a linear describable elastic deformation with respect to the reference frame, see [7, 12]. The equations of motion for a free elastic multibody system read as

$$\mathbf{M}(\mathbf{z}_F)\dot{\mathbf{z}}_{II} = \mathbf{h}_e(\mathbf{z}_F) + \mathbf{h}_\omega(\mathbf{v}, \boldsymbol{\omega}, \mathbf{z}_F, \dot{\mathbf{z}}_F) + \mathbf{h}_a, \quad (1)$$

$$\dot{\mathbf{z}}_{II} = [\dot{\mathbf{v}} \quad \dot{\boldsymbol{\omega}} \quad \dot{\mathbf{z}}_F]^T, \quad (2)$$

where the nodal displacements of the FE structure are denoted by $\mathbf{z}_F \in \mathbb{R}^n$, $\mathbf{z}_{II} \in \mathbb{R}^{6+n}$ are generalized velocities, and n is the number of elastic degrees of freedom. The matrix $\mathbf{M} \in \mathbb{R}^{(6+n) \times (6+n)}$ is the mass matrix, $\mathbf{h}_\omega \in \mathbb{R}^{6+n}$ are generalized inertial forces due to the relative description with respect to the floating frame of reference, $\mathbf{h}_e \in \mathbb{R}^{6+n}$ are generalized forces resulting from elastic body deformations, $\mathbf{v} \in \mathbb{R}^3$ and $\boldsymbol{\omega} \in \mathbb{R}^3$ are the translational and the rotational velocity of the reference system, respectively. All other applied forces and torques, including contact forces, are summarized in $\mathbf{h}_a \in \mathbb{R}^{6+n}$. For the description of the elastic part, most often an FE model is used. Although this allows a precise geometrical discretization, in addition it typically yields a large number of elastic degrees of freedom. In order to reduce the number of degrees of freedom, modal reduction is applied.

Modal reduction

In general, the linear equations of motion for an FE model read

$$\mathbf{M}_F \ddot{\bar{\mathbf{z}}}_F + \bar{\mathbf{K}}_F \bar{\mathbf{z}}_F = \bar{\mathbf{h}}_F, \quad (3)$$

where $\bar{\mathbf{z}}_F \in \mathbb{R}^N$ is the vector of nodal displacements, $\bar{\mathbf{M}}_F \in \mathbb{R}^{N \times N}$ is the mass matrix, $\bar{\mathbf{K}}_F \in \mathbb{R}^{N \times N}$ represents the stiffness matrix and $\bar{\mathbf{h}}_F \in \mathbb{R}^N$ are the applied forces. The matrices $\bar{\mathbf{M}}_F$ and $\bar{\mathbf{K}}_F$ are constant. Even though many different model reduction techniques exist, see [12],

the approach used in this study is the simple modal reduction. It is the basic idea of the modal formulation to use a reduced basis of shape functions, defined by a small number of $n \ll N$ eigenvectors of the associated generalized eigenvalue problem. The N nodal displacements $\bar{\mathbf{z}}_F$ are then approximated by

$$\bar{\mathbf{z}}_F \approx \Phi_{red} \mathbf{q}_{red}, \quad (4)$$

where $\Phi_{red} \in \mathbb{R}^{N \times n}$ is the modal matrix, comprised of the first n eigenmodes of the finite element structure and $\mathbf{q}_{red} \in \mathbb{R}^n$ are the reduced elastic coordinates. The eigenvalues ω_i and the associated eigenmodes φ_i are derived from solving the eigenvalue problem $(-\omega_i^2 \bar{\mathbf{M}}_F + \bar{\mathbf{K}}_F) \varphi_i = \mathbf{0}$. The eigenmodes are chosen mass-orthonormal which results in an identity matrix for the reduced mass matrix $\bar{\mathbf{M}}_{F,red} \in \mathbb{R}^{n \times n}$. The reduced stiffness matrix then becomes a diagonal matrix $\bar{\mathbf{K}}_{F,red} = \text{diag}(\omega_1^2, \dots, \omega_n^2)$.

2.2. Contact algorithm

To calculate the contact forces, a general node-to-surface approach is used, see [9]. During normal operation with large rotational angles each flank may come into contact with many different flanks of the opposite gear. A collision detection looping over all flanks would be possible but is very expensive, since a transformation from modal coordinates to nodal coordinates for every flank node would be needed despite the fact that for geometrical reasons only a small number of flanks are in contact at the same time. To reduce the possible contact nodes, and thus the numerical cost for the transformation, a coarse collision detection is used, see [13].

Coarse collision detection

The coarse collision detection is based on index nodes. Each tooth of a gear is referenced by an index node that is located in the center of each tooth. The absolute positions of the index nodes are calculated in every integration step. The closest index node to the center of the opposite gear is determined and called the instantaneous center node. Based on this center node, a small number of teeth on the left and right are considered as possible contact candidates, see Fig. 1.

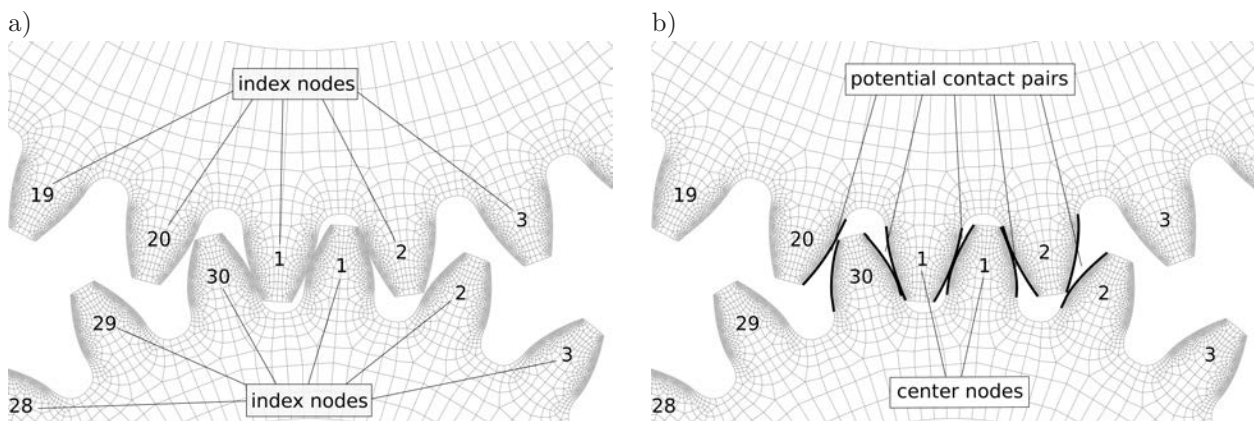


Fig. 1. Coarse contact detection using index nodes (a) and contact candidates (b).

The coarse collision detection reduces not only the number of possible contact nodes but also the size of the transformation matrix, which is needed to transform from modal coordinates to nodal coordinates. The transformation matrix is only updated if the center node changes. Therefore, in each integration step, only the index nodes and the currently valid transformation matrix of the contact candidates have to be stored in memory.

Fine collision detection

The contact between two flanks will be described using a fine collision detection based on a master/slave contact formulation. The two contact partners are separated into a master and a slave element. In a pure master/slave contact formulation, only the penetration of slave nodes into the master elements are considered. Therefore, the main task of the fine collision detection is to find the contact point of the slave node Q on the master surface $P_1P_2P_3P_4$ of the master element as shown in Fig. 2.

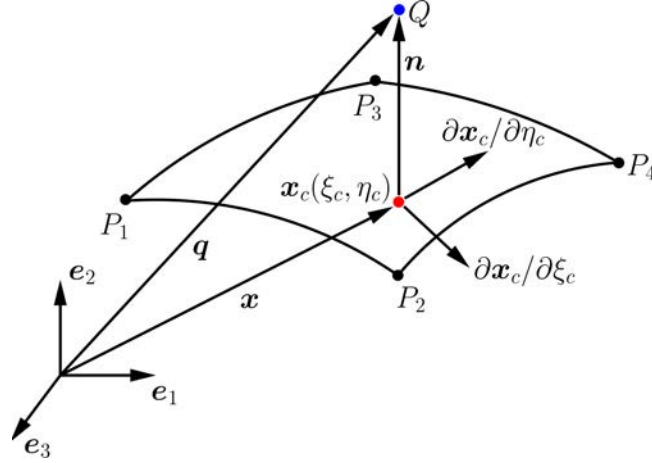


Fig. 2. Fine contact determination.

By using linear hexahedral elements for the discretization of both contact partners, the shape function of the contact surfaces reads

$$\mathbf{x}(\xi, \eta) = \frac{1}{4} \sum_{i=1}^4 (1 + \xi_i \xi)(1 + \eta_i \eta) \mathbf{z}_{F,i}, \quad \xi_i, \eta_i \in [\pm 1], \quad (5)$$

where ξ and η are parameters, ξ_i and η_i are element boundaries and $\mathbf{z}_{F,i}$ are node coordinates of the four master nodes.

Based on the node-to-surface contact, the contact point on the master surface can be found by solving the equations

$$\frac{\partial \mathbf{x}^T}{\partial \xi}(\xi_c, \eta_c) [\mathbf{q} - \mathbf{x}(\xi_c, \eta_c)] = 0, \quad (6)$$

$$\frac{\partial \mathbf{x}^T}{\partial \eta}(\xi_c, \eta_c) [\mathbf{q} - \mathbf{x}(\xi_c, \eta_c)] = 0. \quad (7)$$

A Newton-Raphson iteration is used to solve Eqs. (6) and (7). The penetration g_n of the slave node Q with coordinates \mathbf{q} into the master surface is calculated as

$$g_n = \mathbf{n}^T (\mathbf{x}(\xi_c, \eta_c) - \mathbf{q}), \quad (8)$$

$$\mathbf{n} = \frac{\mathbf{x}_{,\xi}(\xi_c, \eta_c) \times \mathbf{x}_{,\eta}(\xi_c, \eta_c)}{\|\mathbf{x}_{,\xi}(\xi_c, \eta_c) \times \mathbf{x}_{,\eta}(\xi_c, \eta_c)\|}, \quad (9)$$

where \mathbf{n} is the unit normal vector of the contact point \mathbf{x}_c .

When the penetration of the slave node is determined, the nodal contact force can be calculated using a penalty approach. Then, the nodal contact force for the slave node follows directly from its penetration. The nodal contact forces acting on the four master nodes, representing the master

surface, follow from the participation factors of the contact point according to the shape function and the contact point coordinates ξ_c and η_c .

For $g_n \leq 0$, there exists a contact. Following the penalty approach with a penalty parameter c_p , the nodal contact force can be determined as $f_c = c_p |g_n(\xi_c, \eta_c)|$, $g_n \leq 0$. The nodal contact force acting in the direction of the normal vector of the contact point can be calculated by $\mathbf{f}_c = \mathbf{n} f_c$. When all nodal contact forces are determined, the overall nodal contact force vector can be assembled and transformed to the generalized coordinates of the EMBS.

3. SIMULATION

In this section, the fully elastic approach is applied to simulate the contact forces and contact characteristics of straight beveloid gears. Before being applied to beveloid gears, the approach will be applied to a very fine model of a helical gear pair for verification purposes.

3.1. Involute helical gear pair

Involute gears are widely applied in industry because of advantages in design and their simplicity of manufacturing. The contact characteristics of involute gears are very well known. In this section, to verify the approach, a numerical example is presented to demonstrate the application of the presented method for an analysis of contact forces and contact patterns of involute helical gears. The essential gear data are listed in Table 1.

Table 1. Involute helical gear pair.

	pinion	large gear
number of teeth	$z_1 = 18$	$z_2 = 37$
face width	$b_1 = b_2 = 10$ mm	
root fillet radius	$\rho_{a1} = \rho_{a2} = 0.25$ mm	
normal pressure angle	$\alpha_n = 20^\circ$	
normal module	$m_n = 2$ mm	
helical angle	$\beta = 8^\circ$	

For the contact calculation, all the teeth flanks of the gear pair will be very fine discretized with the smallest element edge of about 0.063 mm. The model consists of about 1 200 000 nodes and about 1 000 000 elements. The following results were obtained from the modally reduced elastic multibody model for both gears. As shown in [13], in a modally reduced elastic multibody model, the number of eigenmodes up to an eigenfrequency of about 80 kHz is necessary to get precise results. To fulfill the criterion, 200 eigenmodes for the pinion and 500 eigenmodes for the large gear are used. A driving torque of 50 Nm is applied to the pinion and a braking of about 100 Nm is applied to the large gear.

Figure 3 presents the contact forces and rotational velocities of the gear pair during meshing. Each color line in the Fig. 3 (left) presents a contact force of a tooth pair from going into to going out of contact. Figure 4 shows the contact patterns during meshing at some specific simulation time points.

During meshing, as shown in Fig. 3, the contact changes from double-teeth contact to single-teeth contact and vice versa. Figure 4a presents contact patterns at the very beginning of double-teeth contact, while Fig. 4b at the middle, Fig. 4c at the end of double-teeth contact and Fig. 4d shows the contact pattern of single-teeth contact stage. Theoretically, helical gears have contact patterns starting at a point and then extending to a line-contact, with the line being included by the helical angle. This phenomenon agrees very well with Fig. 4. Besides, the contact lines are enlarged to

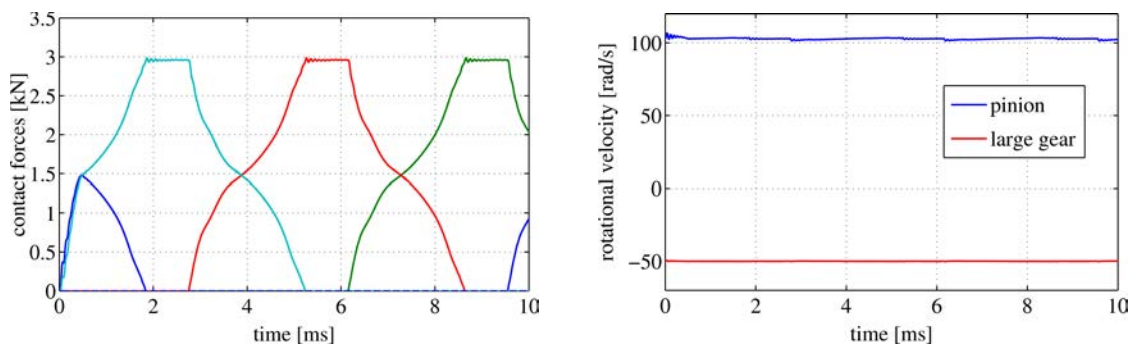


Fig. 3. Contact forces and rotational velocities during meshing.

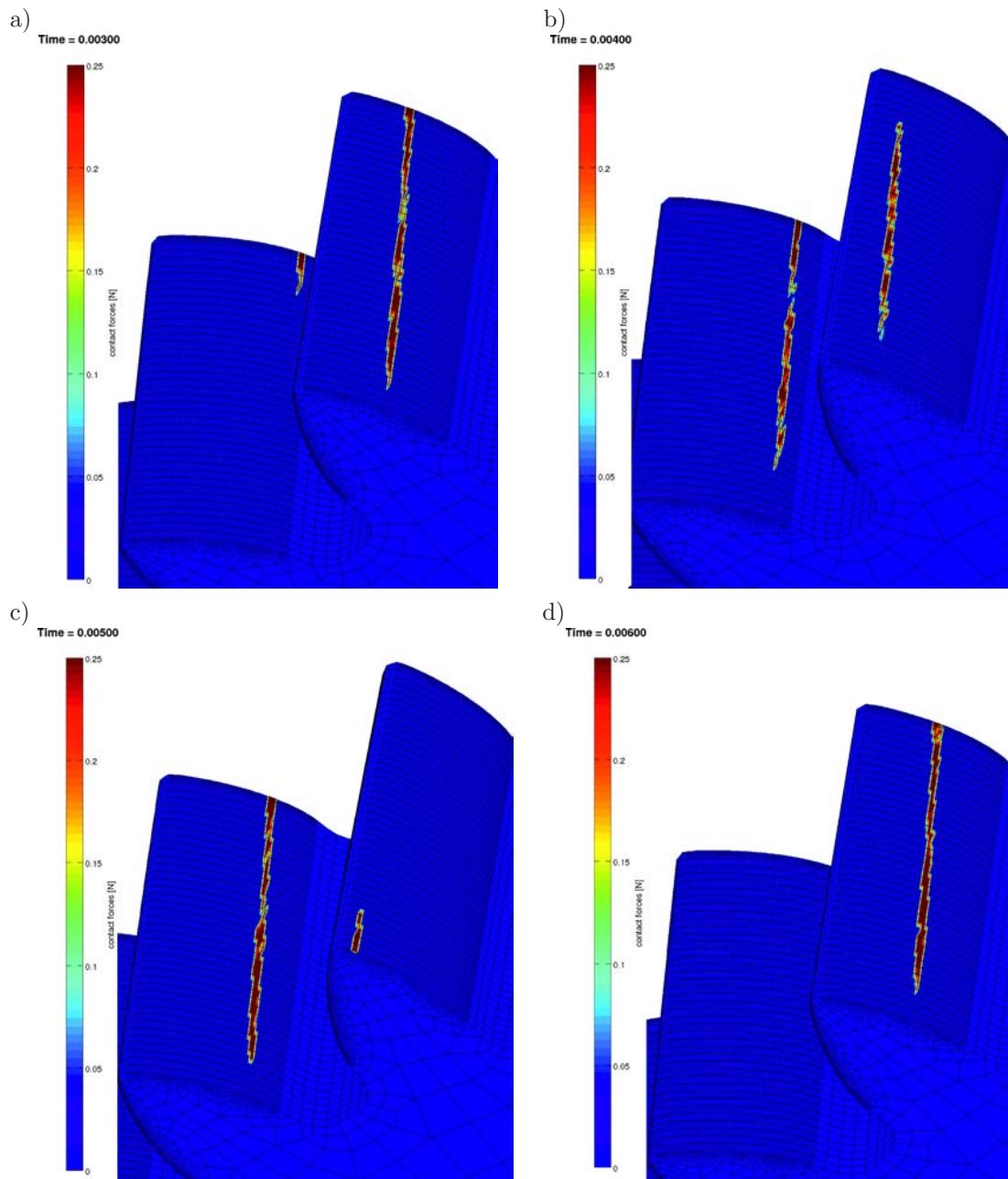


Fig. 4. Contact patterns on the pinion at $t_a = 3$ ms (a), $t_b = 4$ ms (b), $t_c = 5$ ms (c) and $t_d = 6$ ms (d) of simulation time.

contact patterns because of tooth bending deflection and elastic deformations considered by the proposed method.

3.2. Beveloid gear pair

The aim of this study is to propose an efficient approach for loaded gear contact analysis of involute conical gear drives with approximate line contact. For beveloid gears, many studies detailing their geometry, design, manufacturing and inspection have appeared. However, one of the weakest points of beveloid gears is less surface durability in applications due to point contact problems, although the transmission is not correspondingly sensitive to assembly error. In this section, the main topic that requires study is the contact characteristics of beveloid gear drives under different loading conditions. A straight beveloid gear pair, see Fig. 5, with essential gearing data listed in Table 2 will be studied. All the beveloid gear models in this study are supplied by the Institute for Engineering and Industrial Design, University of Stuttgart. The contact characteristics will be studied in four different stages, a new tooth pair going into contact, two tooth pairs equally in contact, then the old tooth pair going out of contact and the new tooth pair going to single-teeth contact.

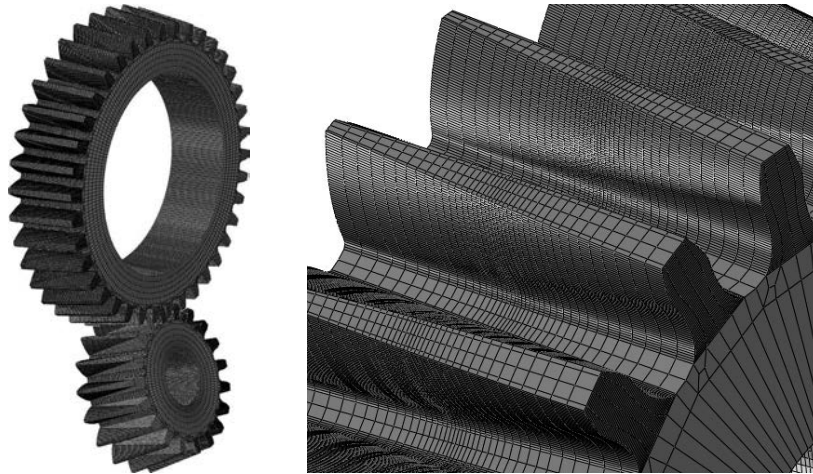


Fig. 5. Straight beveloid gear pair and its non-standard flank profiles.

Table 2. Beveloid gear pair.

	gear 1	gear 2
number of teeth	$z_1 = 19$	$z_2 = 38$
face width	$b_1 = b_2 = 20$ mm	
conical angle	$\theta_1 = \theta_2 = 10^\circ$	
helical angle	$\beta_1 = \beta_2 = 0^\circ$	
profile offset of tooth	0	
root fillet radius, ρ_{fP}	0.25 mm	
normal pressure angle	$\alpha_n = 20^\circ$	
normal module	$m_n = 2$ mm	
intersected angle of shaft	$\Sigma = 20^\circ$	
head clearance coefficient	$c_a = 0.2$ mm	

Since the flank profiles are highly complex, the teeth must be discretized fine enough in both directions of the flank, i.e., the flank width and the face width. The theoretical contact point

normally occurs at the middle of the tooth flank, so the discretization is finer in the middle of tooth flanks. The FE model of the beveloid gear pair consists of about 630 000 nodes and 450 000 elements, with the smallest element edge in the contact areas of about 0.12 mm. A hexahedral element with reduced integration is used here. To get precise results, 300 eigenmodes for the small gear and 500 eigenmodes for the large gear are used.

In this work, the penalty parameter is chosen based on the agreement of the proposed method and accurate FE simulations based on several impacts. Here the value 4×10^6 N/m is chosen. For the impact model, the small gear is given an initial rotational velocity and the large gear is fixed. The reason for only investigating a few impacts is that, for longer simulations like constant meshing, a reference solution in terms of full FE simulation is practically impossible due to very long integration times. In addition, Fig. 6 presents simulation results for a few impacts. Figure 6 shows contact forces and rotational velocities. The red and the blue lines describe the results of FE simulation and the elastic multibody simulation, respectively. Each color line in Fig. 6 (left) presents a contact force of a tooth pair during impacts. In each impact there are always two tooth pairs in contact at the same time. The impact results of both approaches match very well in shape, magnitude and the number of teeth in contact. This indicates that the proposed method is reliable and precise. Later in this work it will be shown that this approach is also much more efficient than a full FEA.

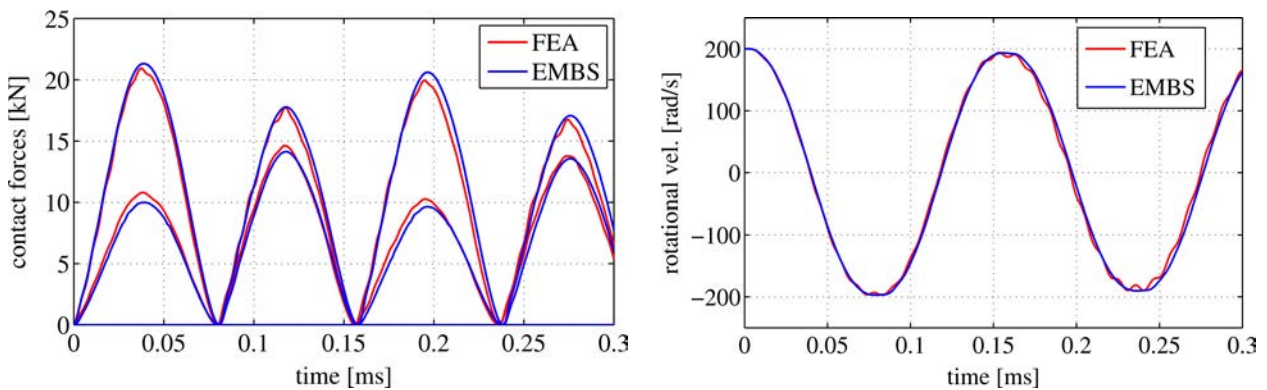


Fig. 6. Contact forces and rotational velocities of several impacts.

Contact characteristics of the beveloid gear pair will be studied under three different loading cases: slight, middle and large braking torque of 20, 100 and 400 Nm, respectively. Figure 7 shows the rotational velocity of the large gear for all load cases. Under the effect of deformations, in all the studied cases the gear was vibrating, especially when a new tooth pair comes into contact. The velocity changes very clearly in case of a very large braking torque of about 400 Nm applied to the large gear because of tooth bending deflection and elastic deformations.

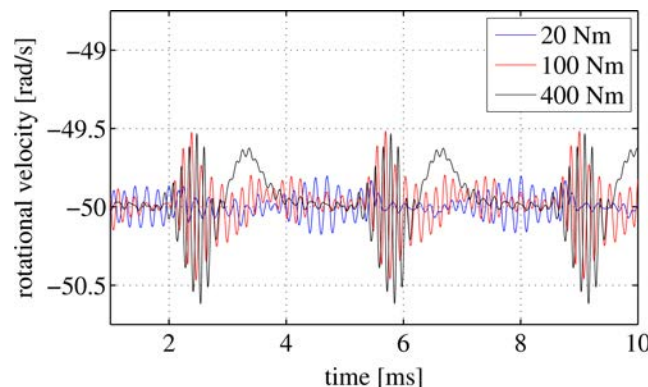


Fig. 7. Rotational velocity of the large gear with different braking torques.

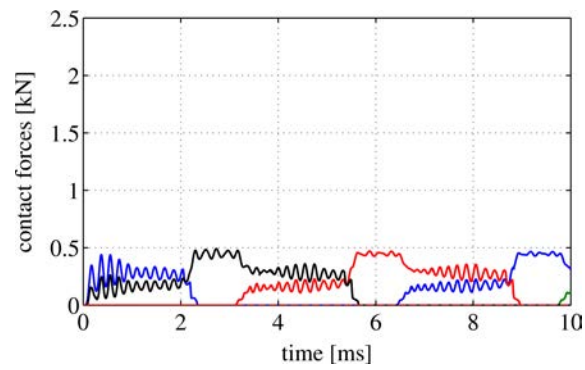


Fig. 8. Contact forces for the beveloid gear pair with a braking torque of 20 Nm applied to the large gear.

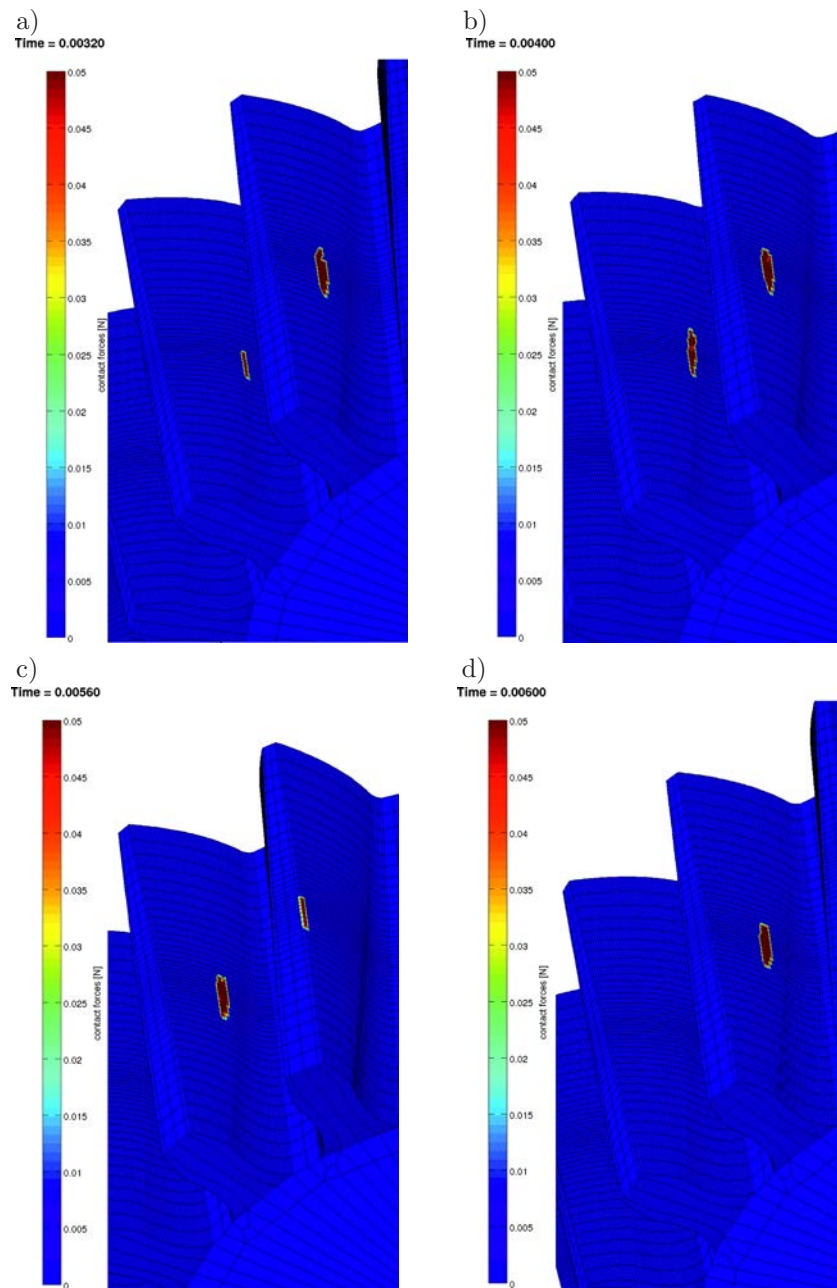


Fig. 9. Contact patterns on the small gear for the gear pair with a braking torque of 20 Nm applied to the large gear.

In the case of 20 Nm, the gears are very sensitive to vibration because of small deformation forces, this leads to the sensitive vibrations of contact forces around their magnitudes, see Fig. 8. Each line in Fig. 8 presents a contact force of a tooth pair during meshing. The colors in Fig. 8 have a different meaning as in Fig. 7. Figure 9 presents contact patterns on the small beveloid gear. Under elastic deformations, the contact patterns are enlarged to ellipses but are still very small. The weak spots of the beveloid gears, the point contact problems, are presented very clearly in Figs. 9a–9d. The colormap describes the contribution of nodal contact forces of nodes in contact regions. The blue color presents areas without contact force, while red color depicts maximum contact force patterns. Contact forces between zero and maximum linearly map to the current colormap of the range from blue to red.

Contact patterns when a new tooth pair comes into contact are described in Fig. 9, Fig. 9b presents two tooth pairs equally in contact, then the old tooth pair going out of contact is presented in Figs. 9c and 9d shows the contact regions when the new tooth pair is going to a single-teeth contact stage.

When the loading torque is enlarged to a medium value of 100 Nm applied to the large gear, the contact forces increase. The teeth remain in contact for a longer time and the single-teeth contact stage is shorter because of elastic deformations and tooth bending deflection, see Fig. 10. As in Fig. 8, contact force oscillations can be observed. These oscillations are caused by two effects. First, by non-smooth approximation of the master surface, but by far the more significant effect is the change of number of interacting teeth during meshing. Therefore, for higher loads, higher oscillations are observed.

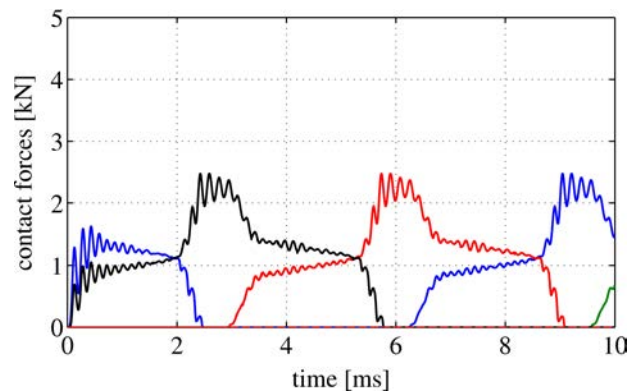


Fig. 10. Contact forces for the beveloid gear pair with a braking torque of 100 Nm applied to the large gear.

Figure 11 presents contact patterns of the medium load case, from a new tooth pair going into contact of a double-teeth contact stage to this new tooth pair going to a single-teeth contact stage. Together with the increasing of contact forces, the ellipses of contact patterns are also enlarged, see Figs. 11a–11d, yet the contact ellipses are still small.

In the case of very high loads with a braking torque of 400 Nm applied to the large beveloid gear and a driving torque of 200 Nm applied to the small gear, Fig. 12 shows more tooth bending deflection and elastic deformations. Under the effect of the deformations, the teeth stay longer in contact, since there are practically two tooth pairs simultaneous under load. Contact patterns are shown in Fig. 13. The contact ellipses in the loading case are certainly more enlarged but still relatively small with about 30% of the tooth flank width. On the other hand, although nearly two teeth pairs are always concurrently in contact, the colormap shows that the contact pressure in the contact regions is very high, see Fig. 13.

The elastic deformations are also influencing the transmission ratio and the accuracy of transmission. Figure 14 presents the transmission ratio of the beveloid gear pair for different load cases. The plot shows that the larger elastic deformation leads to a reduced accuracy of transmission. A perfect transmission would be a constant value, i.e., a straight horizontal line.

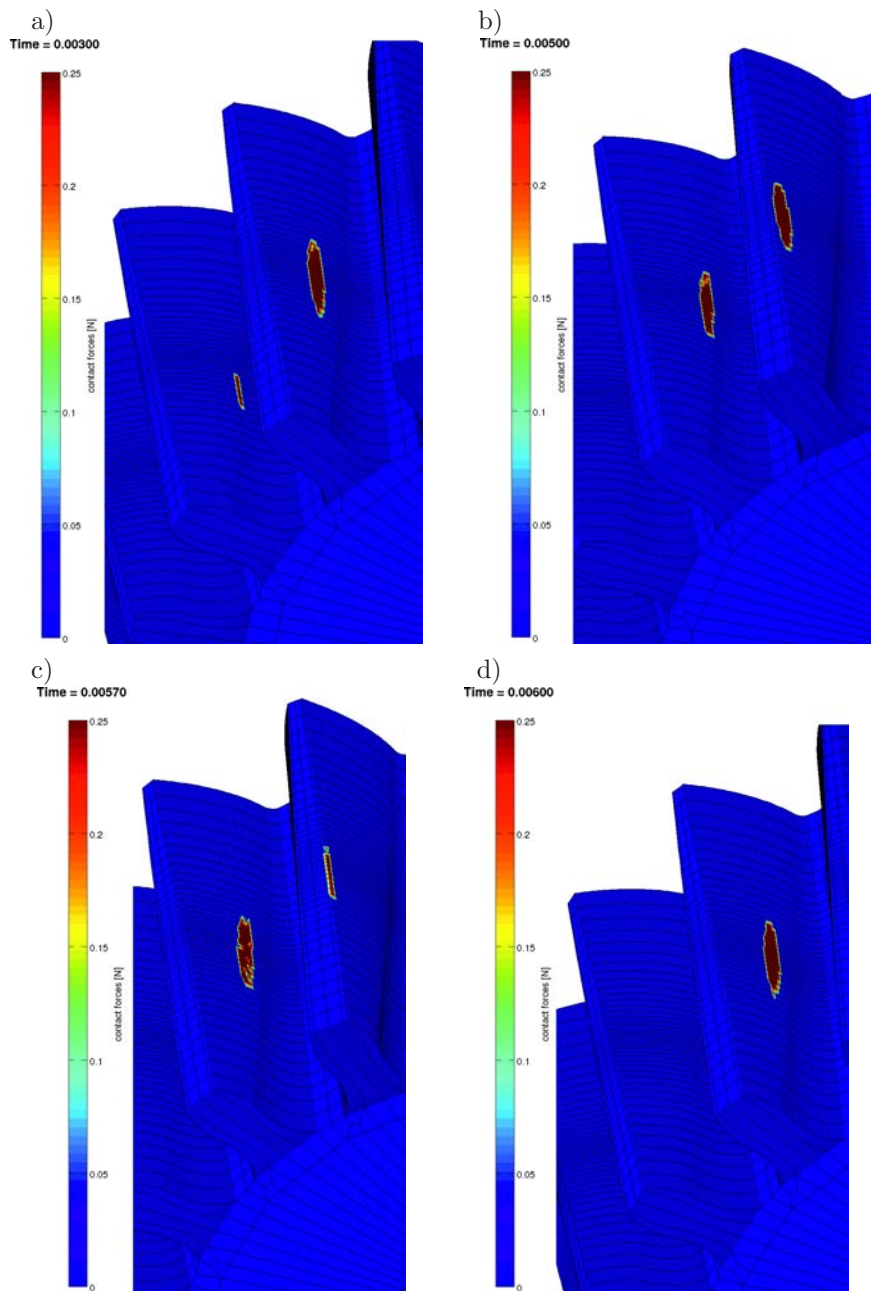


Fig. 11. Contact patterns on the small gear for the gear pair with a braking torque of 100 Nm applied to the large gear.

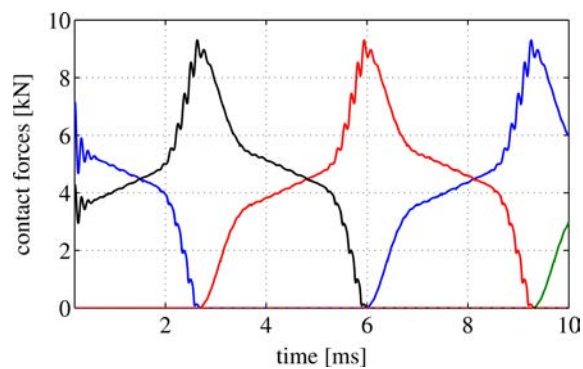


Fig. 12. Contact forces for the beveloid gear pair with a large braking torque of 400 Nm applied to the large gear.

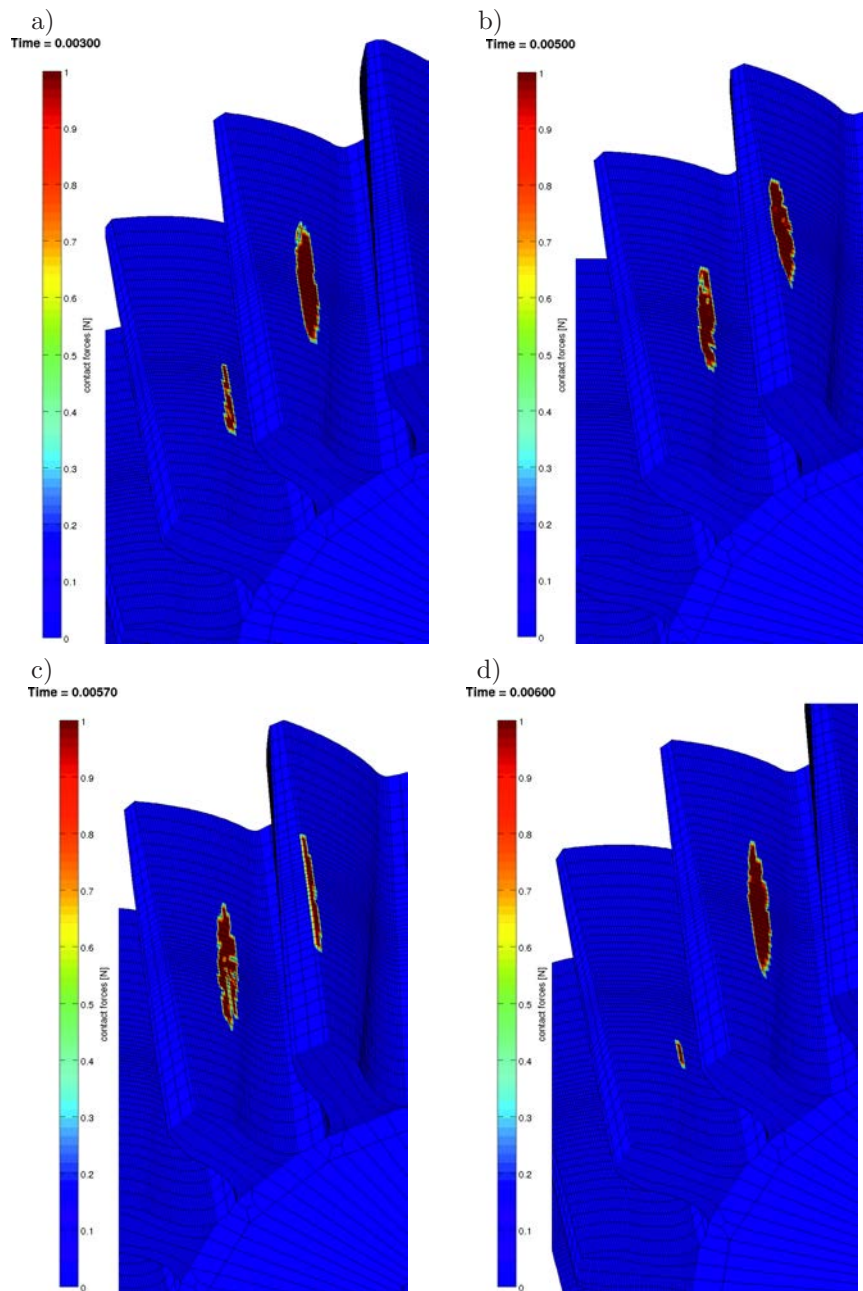


Fig. 13. Contact patterns on the small gear for the gear pair with a large braking torque of 400 Nm applied to the large gear.

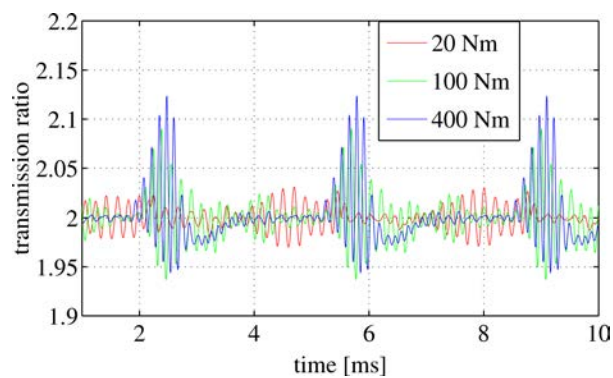


Fig. 14. Transmission ratio of the beveloid gear pair with different braking moments.

The results of this numerical example confirm the weak spot of beveloid gears, the contact point problem. It also presents the effects of elastic deformations of fully elastic bodies and their influence on the contact patches and their transmission accuracy. To overcome these weak points, the beveloid gears need to be corrected or optimized. In the next section, a solution will be introduced and studied.

3.3. Beveloid and spur gear pair

The behavior of beveloid gears is not as well understood as the behavior of spur or bevel gears. Analyses of their behavior are often limited to an analytical rigid point contact [2] or a very small contact range of tooth flanks during meshing [6]. The increasing interest in beveloid gears is mainly based on their positive attributes. They are not as sensitive against mountings errors as involute gear are and they can be used with intersecting, parallel and skew shafts in the same manner as bevel, spur and helical gears. They are frequently deployed for marine transmission, but they are also increasingly important in the automobile industry. Different applications of beveloid gears are cooperating with cylindrical involute gears as seen in Fig. 15, see [14, 15].

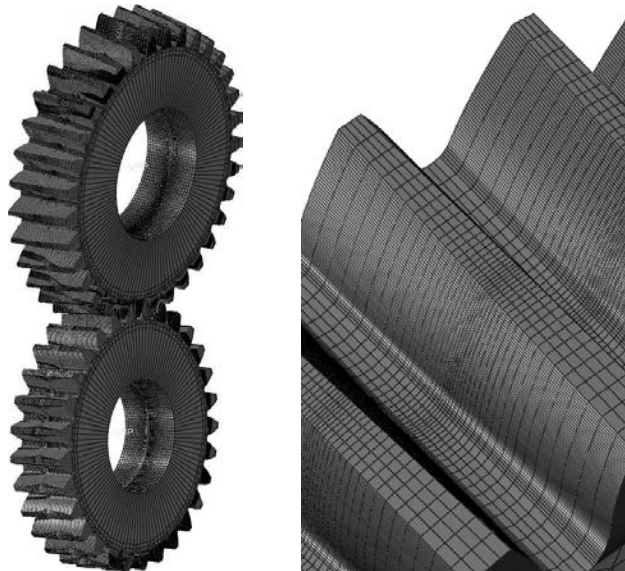


Fig. 15. Beveloid and spur gear pair with non-standard flank profiles of the beveloid gear.

In this section, a gear pair of a straight beveloid gear and a spur gear, supplied by the Institute for Engineering and Industrial Design, University of Stuttgart, will be studied. The major parameters of the gear pair are listed in Table 3. First, contact behaviors of the origin gear pair will be simulated, later they will be compared to behaviors of the corrected gear pair.

On the other hand, the possible combinations of gear models from the Institute for Engineering and Industrial Design are normally verified based on the estimation of load-free gape. The load-free gape of two meshing gears is the shortest distance between an arbitrary point on the gear flank to the opposite gear in a close-fitting and undeformed meshing position. For the beveloid and spur gear pair, the uncorrected gear pair has point contact. When the uncorrected beveloid gear combines with the corrected spur gear, the load-free gape will be reduced by about 10%. When the corrected beveloid gear joins together with the uncorrected spur gear, the load-free gape is reduced by about 75%. When the two corrected gears cooperate, the load-free gape may be reduced up to 85%. This shows that the correction of beveloid gears plays an important role in improving the working ability of the gear pair. In this study, only the combination of two uncorrected and two corrected gears will be investigated and compared.

Table 3. Beveloid and spur gear pair.

	spur gear	beveloid gear
number of teeth	$z_1 = 29$	$z_2 = 33$
conical angle	$\theta_1 = 0^\circ$	$\rho_2 = 11.09^\circ$
distance to intersected point	809.83 mm	809.03 mm
helical angle	$\beta_1 = \beta_2 = 0^\circ$	
face width	$b_1 = b_2 = 30$ mm	
root fillet radius, ρ_{fP}	0.38 mm	
wheel hub width	30 mm	
profile offset of tooth	0.25	
normal pressure angle	$\alpha_n = 20^\circ$	
normal module	$m_n = 4.5$ mm	
intersected angle of shaft	$\Sigma = 10^\circ$	
head clearance coefficient	$c_a = 1.25$ mm	

Uncorrected gear pair

As the investigated beveloid gears in Subsec. 3.2, the teeth of both gears must be discretized fine enough in both directions of the flank, the flank width and the face width. The discretization is finer in the middle of tooth flanks. The FE model of the beveloid and spur gear pair consists of about 700 000 nodes and 540 000 elements, with the smallest element edge in the contact areas of about 0.2 mm. A hexahedral element with reduced integration is used here. To get precise results, 300 eigenmodes are used for both gears. The contact behavior of the gear pair will be studied for two different load cases. First, a small braking torque and then a medium braking moment will be applied to the beveloid gear. Contact patterns are also shown in four different contact situations of a tooth pair.

Figure 16 presents contact forces of the spur gear during meshing. Each line of the plot describes a contact force of one tooth pair from going into to going out of contact. The influence of elastic deformations is presented through the vibrations of contact forces around their magnitudes. Contact behaviors of beveloid gear flanks can be described based on the opposite contact flanks of the spur gear. The contact patterns of the spur gear are shown in Fig. 17. As for the beveloid gear pair in Subsec. 3.2, contact regions occur in the middle of gear flanks and under the elastic deformations of gear the contact regions enlarge to ellipses. However, these contact regions look wider in the flank width direction than the previous beveloid gear pair in Subsec. 3.2.

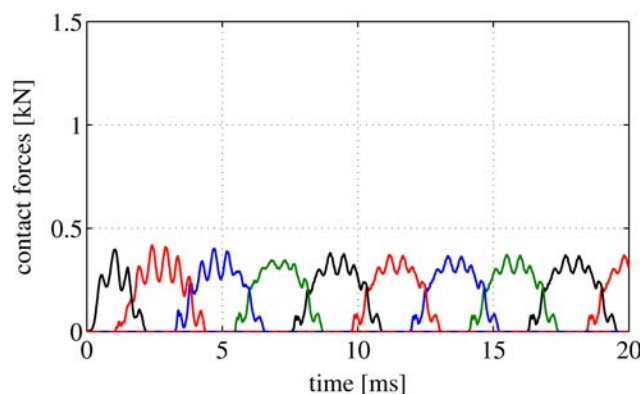


Fig. 16. Contact forces for the beveloid and spur gear pair with a braking torque of about 20 Nm applied to the large gear.

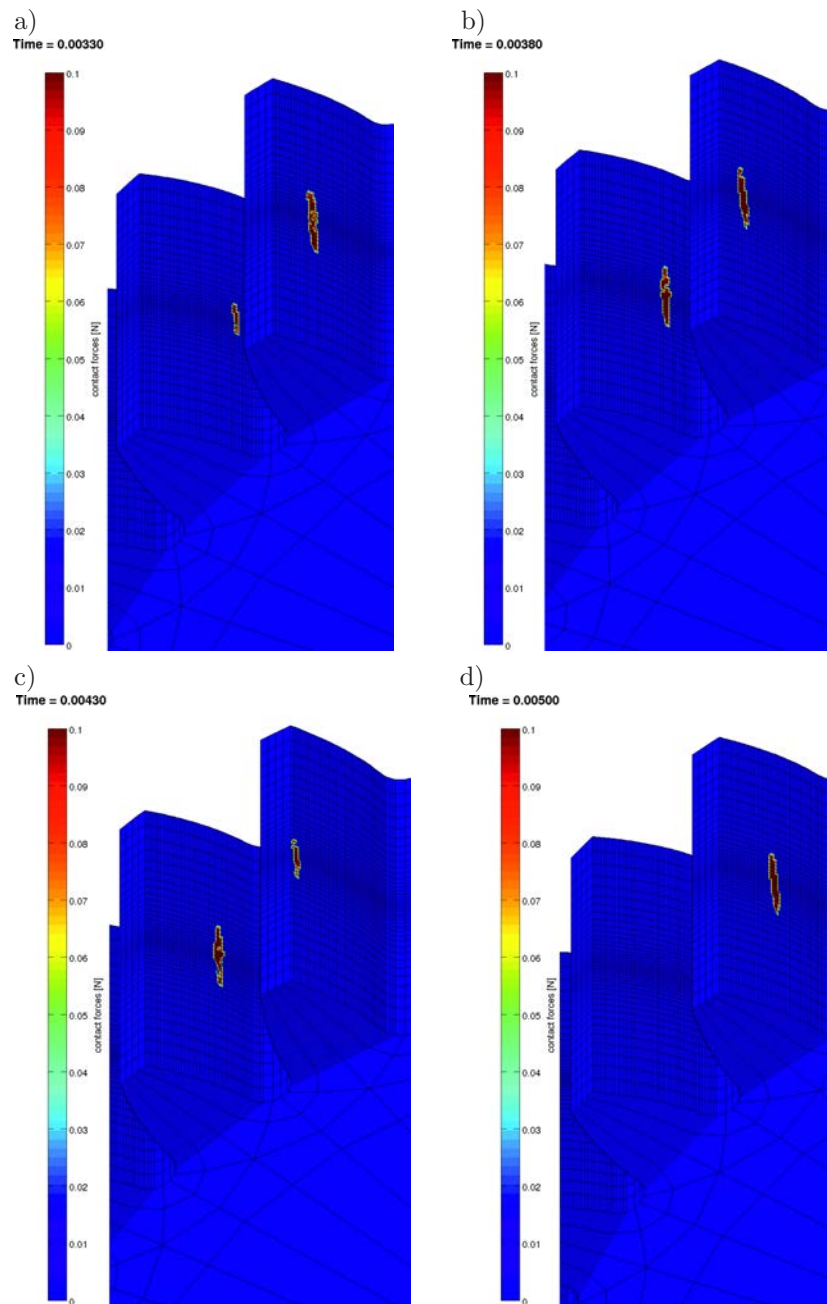


Fig. 17. Contact patterns on the spur gear for the beveloid spur gear pair with a braking torque of about 20 Nm applied to the beveloid gear.

As shown in Fig. 18, under the larger load of 200 Nm, the contact forces are increasing, the teeth remain in contact for a longer time and the single-teeth contact stages are shorter because of larger elastic deformations and larger tooth bending deflections. Besides, the larger deformations and deflections lead to larger backlash between the teeth going into contact. This results in stronger vibration amplitudes when a new tooth pair is going into or going out of contact. The contact patterns are also becoming enlarged because of elastic deformations of the gear flanks, see Fig. 19. Again, the shapes of contact regions shown in Fig. 19 also present a wider contact pattern than of the beveloid gear pair in Subsec. 3.2.

Although the geometry of the gears with normal module of $m_n = 4.5$ mm is much bigger than of the gears in Subsec. 3.2 with normal module of $m_n = 2$ mm, under the medium load case, the

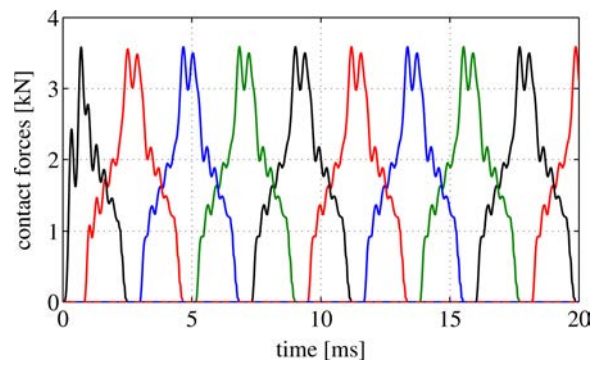


Fig. 18. Contact forces for the beveloid and spur gear pair with a braking torque of about 200 Nm applied to the large gear.

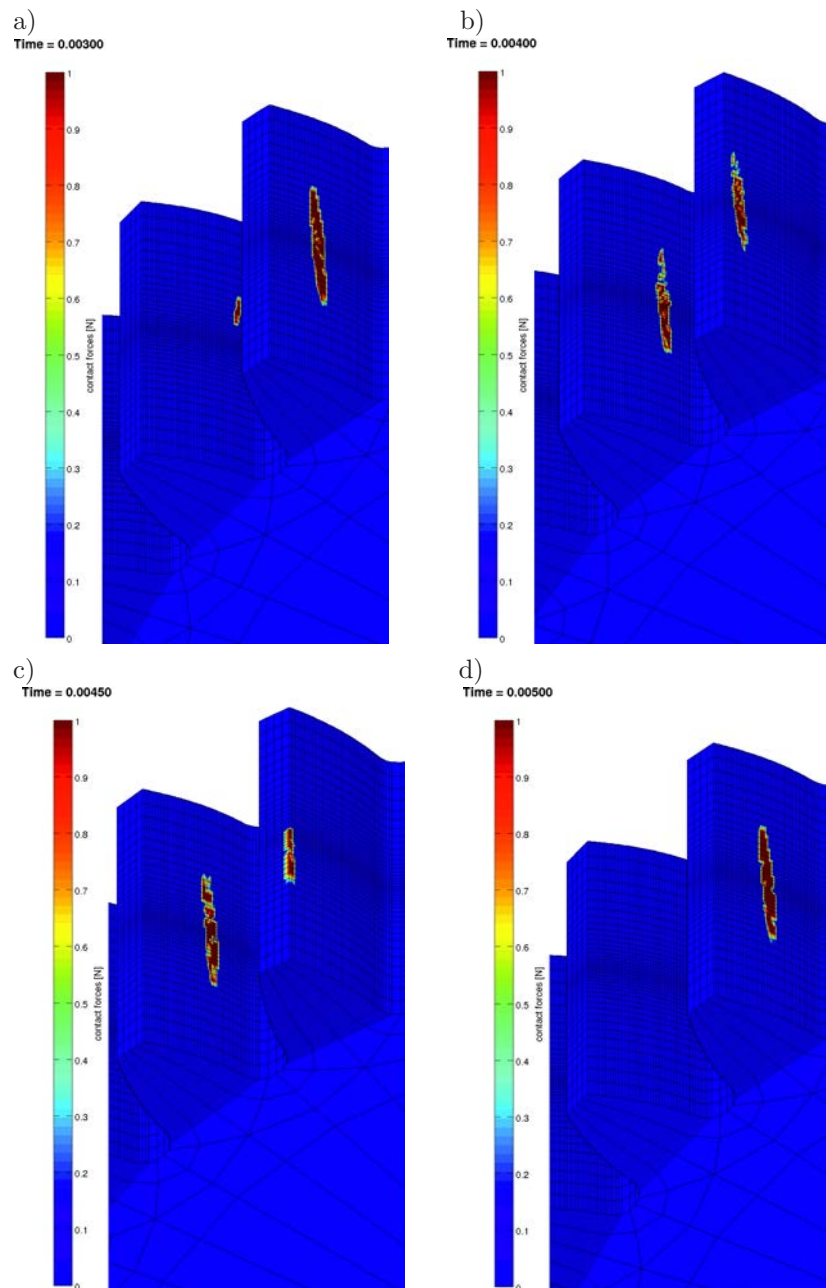


Fig. 19. Contact patterns on the spur gear for the beveloid spur gear pair with a braking torque of about 200 Nm applied to the beveloid gear.

contact ellipses of this gear pair are about 40% of the face width. However, the contact patterns do not satisfy the requirement of approximate line contact.

To optimize the contact behavior, the gears were corrected. The corrections were made based on advice of the Institute for Engineering and Industrial Design, University of Stuttgart. The corrected variations in this situation are tip relief and profile shift correction.

Corrected gear pair

To remedy the disadvantageous characteristic of very small contact pattern, in practice beveloid gear flank are mostly corrected by profile shift of tooth flanks. Such a corrected gear pair will be studied in this section. The FE model of the corrected gear pair also consists of about 700 000 nodes and 540 000 elements. Again, a hexahedral element with reduced integration is used and 300 eigenmodes of each gear are used. For comparison, the setup of the corrected model and the load cases are the same as for the uncorrected gear pair.

Figure 20 presents contact forces of the spur gear during meshing under the small load case with a braking torque of about 20 Nm applied to the beveloid gear. Each line of the plot describes a contact force of one tooth pair from going into to going out of contact. The influence of elastic deformations is also apparent through the vibrations of contact forces.

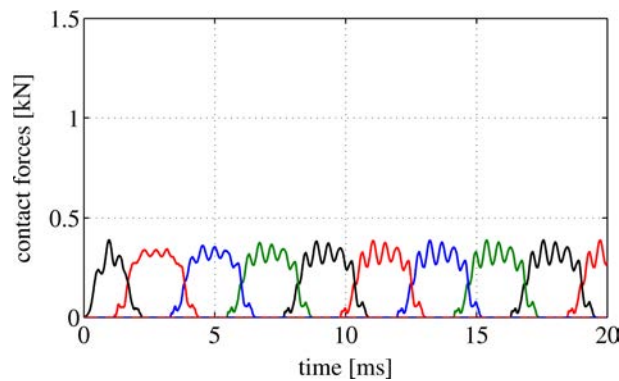


Fig. 20. Contact forces for the corrected beveloid and spur gear pair with a braking torque of about 20 Nm applied to the large gear.

For the small load case, the contact behaviors shown in Fig. 21 depict positive results of the correction. In comparison with the same load case of the uncorrected model in Fig. 16, the corrected gear pair has much wider contact ellipses of about 45% of the face width. It presents the true estimation based on the load-free gape of the attached document. The contact ellipses width increases up to about 90% in comparison with contact ellipses of the uncorrected gear pair, see Figs. 17 and 21.

In case of medium braking moment of about 200 Nm applied to the beveloid gear, the contact forces are increasing, see Fig. 22. The contact forces of a tooth pair from going into to going out of contact are described as a line in the plot.

The contact patterns are also becoming longer because of elastic deformations of gear flanks and the effects of corrections, see Fig. 23. Again, the shapes of contact regions shown in Fig. 23 present a contact behavior as expected. The contact ellipses in a single-teeth contact stage take about 90% of the face width. The quality of contact in this case is also recognized in Figs. 18 and 22 through the reduced vibration of the contact forces. The contact ellipses are enlarged leading to better contact qualities.

Figure 24a also shows the positive results of the correction. The elastic deformation and tooth bending deflection do not only directly influence the quality of contacts but also the quality of transmission. For gears considered as rigid bodies, the transmission ratio is constant, but under

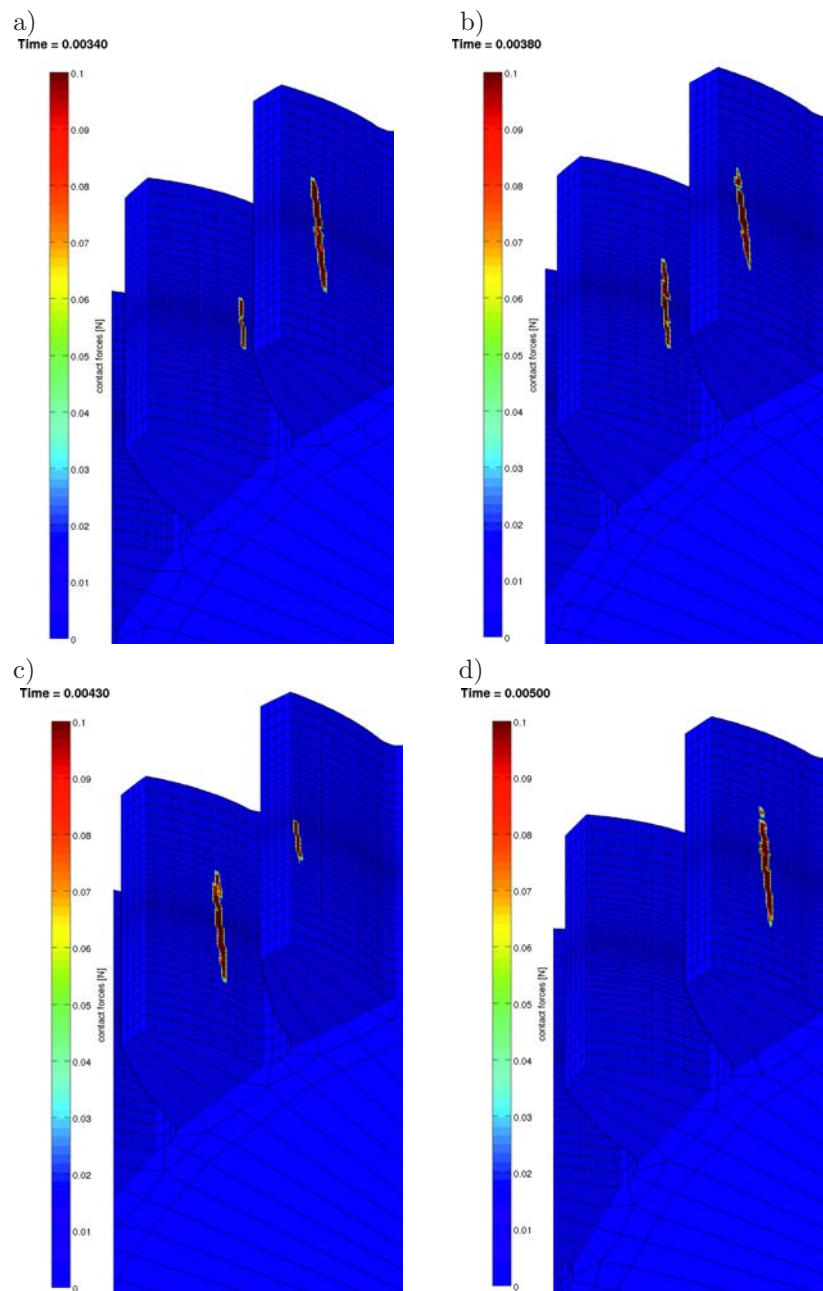


Fig. 21. Contact patterns on the spur gear for the beveloid spur gear pair with a braking torque of about 20 Nm applied to the beveloid gear.

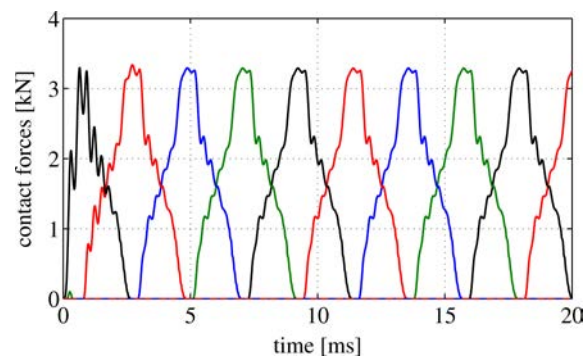


Fig. 22. Contact forces for the corrected beveloid and spur gear pair with a braking torque of about 20 Nm applied to the large gear.

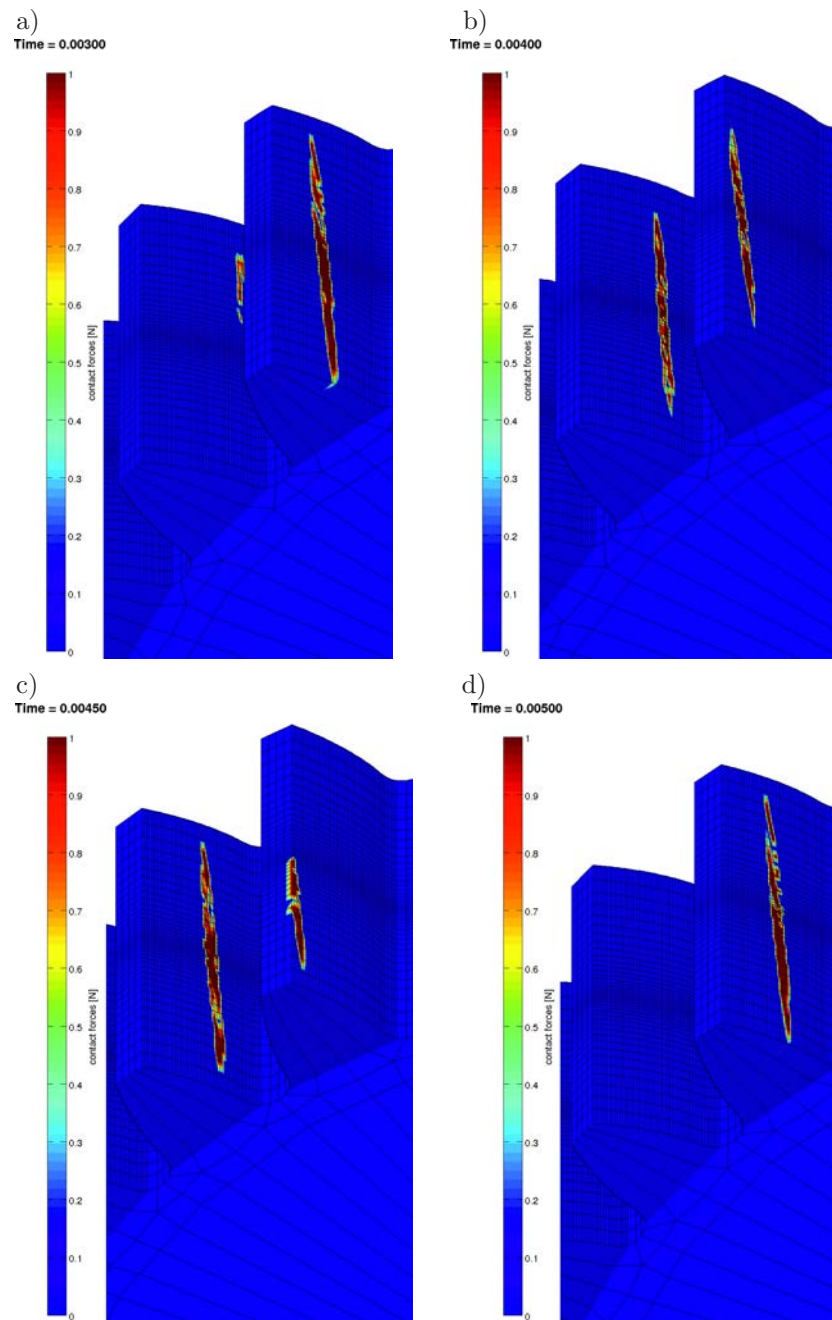


Fig. 23. Contact patterns on the spur gear for the beveloid spur gear pair with a braking torque of about 200 Nm applied to the beveloid gear.

influence deformations the ratio changes during meshing, see Fig. 24b. The larger the load case is, the more the transmission error increases.

Table 4 presents a comparison of the simulation models used for the results presented in Fig. 6 using FEM and EMBS. The contact algorithm and the modal reduction of the approach, see Subsec. 2.2, leads to a tremendous reduction in integration time of the simulation. However, the EMBS requires a preprocessing step to solve the eigenvalue problem and to compute the standard input data for the reduced EMBS. This may be numerically very expensive, but has to be calculated only once. All following simulations use this standard input data. Therefore, this approach practically benefits if many subsequent simulation or long simulations are required as in the case of many revolutions.

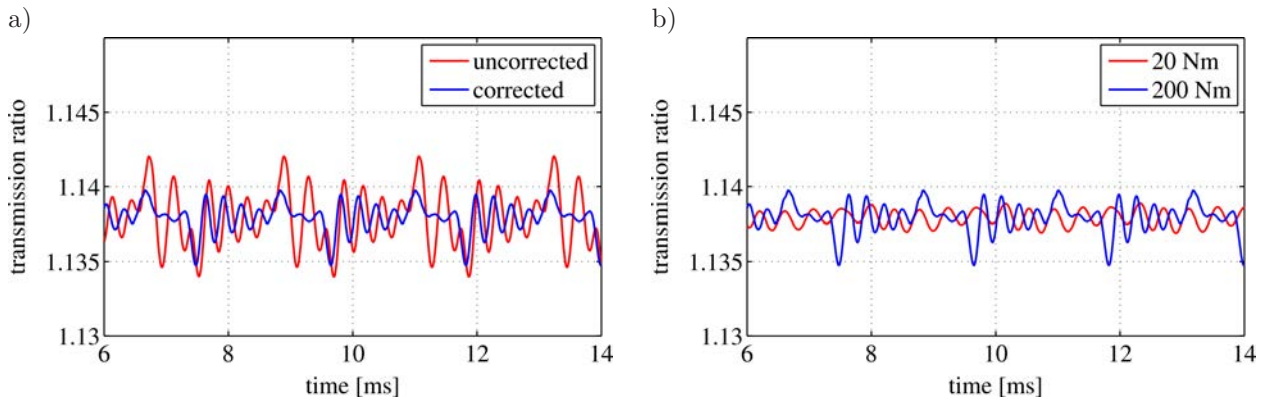


Fig. 24. Transmission ratio of the beveloid spur gear pair before and after correction with braking moment of 200 Nm applied to the beveloid gear (a) and transmission ratio of the corrected beveloid spur gear pair with different braking moments (b).

Table 4. Integration time, disk and memory requirement for impact investigations on the beveloid gear pair for four impacts for FE model and elastic multibody model using the same computer (Intel Core i7-2600, 3.40 GHz, 8 Cores and 32 GB RAM).

model	preprocess	integration time	disk requirement	memory requirement
FEM	0 h	8738 s	≈ 2.6 GB	≈ 1.4 GB
EMBS	24 h	857 s	≈ 10.3 GB	≈ 0.76 GB

Figure 25a presents contact forces in a simulation of about two revolutions of the spur gear, while Fig. 25b shows a zoom into a detail of Fig. 25a.

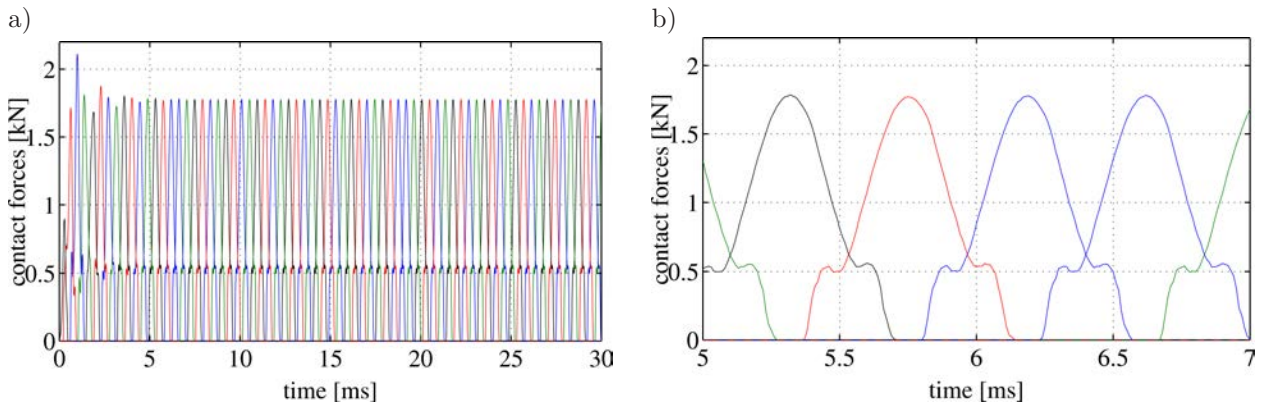


Fig. 25. Contact forces of a simulation with multi revolutions of the spur gear (a) and a zoom during a short stage (b).

4. CONCLUSION

According to the proposed method, not only we can obtain the contact forces, but also the shape of contact patterns of helical involute gears and beveloid gears. The influence of elastic deformations and tooth bending deflections in contact regions and contact forces are presented. It shows that these deformations and deflections have direct effect on the distribution of contact patterns. This is especially important for the gear drives with involute conical gears, because the tooth surface stress has a direct effect on the durability of drives.

For the purpose of applying the fully elastic multibody method for beveloid gears, a very fine model of an involute helical gear pair was studied for verification. Then the method was applied

to a beveloid gear pair. Accordingly, a very good agreement between FE method and the proposed approach was presented. Moreover, the change in contact force and contact pattern for different load cases was discussed. The results agree very well with the industrial knowledge that the corrections lead to more equally distributed contact forces and therefore to an increased durability.

To depict the improvement of tooth surface durability after correction of beveloid gears, another pair of a straight beveloid gear and an involute spur gear with and without correction was studied by the proposed approach. The simulation results have demonstrated the right theory of correction approach. Compared to classical approaches that are based on analytical rigid body models, one major advantage of the approach proposed in this work is that it allows to include the full deformation in a fully transient time simulation, i.e., under realistic load situation. Furthermore, it was shown that the fully elastic multibody approach is very reliable and more efficient for contact analyses of gear drives, especially for the simulation of multiple revolutions of gears.

REFERENCES

- [1] C. Zhu, H. Wang, L. Zhang, T. Peng. Contact characteristics of helical conical gears used for V-drive marine transmissions. *Proceedings of the Institution of Mechanical Engineering Science Part C: Journal of Mechanical Engineering Science*, **225**(1): 216–224, 2010.
- [2] C.C. Liu, C.B. Tsay. Contact characteristics of beveloid gears. *Mechanism and Machine Theory*, **37**: 333–350, 2002.
- [3] Y.C. Chen, C.C. Liu. Contact stress analysis of concave conical involute gear pairs with non-parallel axes. *Finite Elements in Analysis and Design*, **47**: 443–452, 2011.
- [4] S.H. Wu, S.J. Tsai. Contact stress analysis of skew conical involute gear drives in approximate line contact. *Mechanism and Machine Theory*, **44**: 1658–1676, 2009.
- [5] C.C. Liu, Y.C. Chen, S.H. Lin. Contact stress analysis of straight concave conical involute gear pairs with small intersected angles. *Proceedings of the International MultiConference of Engineers and Computer Scientists 2010* Vol. III, IMECS, Hong Kong, March 17–19, 2010.
- [6] C.C. Liu, C.B. Tsay. Mathematical models and contact simulations of concave beveloid gears. *Journal of Mechanical Design*, **124**: 753–760, 2002.
- [7] A.A. Shabana. *Dynamics of multibody systems*. University Press, Cambridge, 1998.
- [8] R. Schwertassek, O. Wallrapp. *Dynamik flexibler Mehrkörpersysteme* (in German). Vieweg, Braunschweig, 1999.
- [9] P. Wriggers. *Computational contact mechanics*. Springer Berlin, 2nd ed., 2006.
- [10] O.A. Bauchau. *Flexible multibody dynamics*. Dordrecht: Springer 2011.
- [11] M. Lehner, P. Eberhard. A two-step approach for model reduction in flexible multibody dynamics. *Multibody System Dynamics*, **17**(2–3): 157–176, 2007.
- [12] K. Sherif, W. Witteveen, K. Mayrhofer. Quasi-static consideration of high-frequency modes for more efficient flexible multibody simulations. *Acta Mechanica*, **223**: 1285–1305, 2012.
- [13] P. Ziegler, P. Eberhard. Simulative and Experimental Investigation of Impacts on Gears Wheels. *Computer Methods in Applied Mechanics and Engineering*, **197**: 4653–4662, 2008.
- [14] C. Brecher, T. Röthlingshöfer, C. Gorgels. Manufacturing simulation of beveloid gears for the use in a general tooth contact analysis software. *Production Engineering Research and Development*, **3**: 103–109, 2009.
- [15] T. Röthlingshöfer. Auslegungsmethodik zur Optimierung des Einsatzverhaltens von Beveloidverzahnungen (in German). Berichte aus der Produktionstechnik (zugl. Dissertation), Schriften aus RWTH Aachen, Band 3. Shaker Verlag, Aachen, 2012.